Rendiconti Lincei. Scienze Fisiche e Naturali (2026) 37 (Suppl 1):S9–S26
https://doi.org/10.1007/s12210-025-01368-8

Climate in a Mediterranean nature reserve: patterns and trends in the Castelporziano Presidential Estate (Italy)

Edmondo Di Giuseppe[1] · Sara Quaresima[1] · Giorgio Matteucci[1] · Carlotta Ferrara[2] · Tiziano Sorgi[2] · Valerio Moretti[2] · Piermaria Corona[2] · Massimiliano Pasqui[1]

Received: 30 May 2025 / Accepted: 9 September 2025 / Published online: 18 March 2026

Abstract
This paper analyzes the seasonal and annual patterns of precipitation and temperature in the Castelporziano Nature Reserve from 1980. It also considers an index that combines precipitation and evapotranspiration. The results indicate various patterns within this small region, primarily influenced by the distance from the coast. Additionally, there is a clear upward trend in temperature. The joint analysis of precipitation and temperature shows that the most recent years have been characterized as either the hottest and driest or the hottest and most humid. Furthermore, there has been a significant increase in tropical nights and a longer duration of warm spells for maximum temperatures.

Keywords Extreme events · Temperature · Precipitation · Spei

1 Introduction

Climate change poses a risk to large parts of Mediterranean regions because of the increase in extreme events, such as heat waves, severe and intense precipitation episodes, or long dry periods (Baldi et al. 2006; Dono et al. 2016; Pasqui and Di Giuseppe 2019; MedECC 2020; IPCC 2023).

In particular, the MedECC (2020) clarified that the Mediterranean region is warming faster than the global average, with critical impacts on water, agriculture, biodiversity, and health. IPCC AR6, in 2023, highlighted, among other risks already identified in earlier reports, the risk of multiple concurrent climate hazards, such as drought and heatwaves. For these reasons, the Mediterranean basin is considered a climate "hotspot" and is among the most vulnerable regions in the World to face the impacts of the climate crisis. Water resources are thus under pressure with an expected reduction in water availability along with an increased water demand and stress, especially for agriculture and urban use, with a high risk of biodiversity loss in all areas. Future projections indicate an increasing risk for extreme events, especially for heatwaves, droughts, and wildfires, even with moderate emission scenarios (IPCC 2023). Hence, there is an urgent

This special issue gathers peer-reviewed articles promoted by the Scientifi c Council of Castelporziano Presidential Estateand supported by the Segretariato Generale della Presidenza della Repubblica as part of the Presidential Decree n.69/N/2020 and subsequent amendments and supplements.

✉ Sara Quaresima
sara.quaresima@cnr.it

Edmondo Di Giuseppe
edmondo.digiuseppe@cnr.it

Giorgio Matteucci
giorgio.matteucci@cnr.it

Carlotta Ferrara
carlotta.ferrara@crea.gov.it

Tiziano Sorgi
tiziano.sorgi@crea.gov.it

Valerio Moretti
valerio.moretti@crea.gov.it

Piermaria Corona
piermaria.corona@crea.gov.it

Massimiliano Pasqui
massimiliano.pasqui@cnr.it

[1] Institute of BioEconomy, CNR, Via dei Taurini 19, 00185 Rome, Italy

[2] Research Centre for Forestry and Wood, CREA, Via Valle della Quistione, 00166 Rome, Italy

need for adaptation, particularly in water management, agro-ecology, forest management, and urban planning.

Urban areas are particularly under the stress of heat waves because of the impacts on a large number of persons in one shot, but also dry periods cause a lack of water reservoirs for the population. Great suffering might also occur in urban vegetation, which is crucial for population stress recovery. Rome is among the urban areas under stress because of climate change. For example, heatwaves have put pressure on the administration to manage health-critical situations due to an unexpected rise in mortality rates (Centers for Disease Control and Prevention 2004; D'Ippoliti et al. 2010). Similarly, the drought crisis of 2017 has caused a water rationing either for civil or economic uses as well as great pressure on the ecosystem of the Bracciano Lake, the major water reservoir for Rome (Sappa et al. 2019; Armenia et al. 2021; Ventura et al. 2023).

The Castelporziano Presidential Estate (CPE) is a large protected area along the Tyrrhenian coast, close to Rome, being almost embedded in its urban context. The area hosts a relevant mosaic of Mediterranean evergreen forests and sub-Mediterranean deciduous formations, but also includes some meso-temperate elements characteristic of Central Europe. While forested areas are the most spread ecosystem type, at CPE there are also dune ecosystems, open areas and wetland ecosystems, with a variety of habitats (Pignatti et al. 2015; Nardone et al. 2025). In this respect, the CPE is of paramount importance for nature and biodiversity conservation, but also for the ecosystem services that it provides to its surroundings, including a large city like Rome. In recent years, some CPE ecosystems are exhibiting signs of decline with potential threats to their long-term sustainability. Therefore, it is fundamental to unravel the possible drivers of the ongoing ecosystem decline. In this respect, climate change is of particular interest, also in consideration of the warming in the Mediterranean area.

This paper presents a climate analysis of the area corresponding to the CPE and a comparison of the climate features and trends with the urban area of Rome. The analysis is done starting from 1980 to avoid including climate regimes that are no more valid in the actual historical period. As a matter of fact, it is demonstrated that, in the Northern Hemisphere, a breakpoint in the regimes of temperature as well as of precipitation is present at the end of '70s. For example, Monteiro and Costa (2023) identified a change point in temperature in the '80. In addition, Panagiotopoulos et al. (2005) identified a dramatic decrease in the Siberian High index between 1978 and 2000, an index that affects atmospheric circulation and temperature patterns in the Northern Hemisphere. Furthermore, the latest Intergovernmental Panel on Climate Change (IPCC) assessment concluded with high confidence that Northern Hemisphere springtime snow water equivalent has "generally declined" since 1981 (Masson-Delmotte et al. 2021). Accordingly, Gottlieb and Mankin (2024) identified a declining snow trend in 82 out of 169 major Northern Hemisphere river basins posing a risk to water resources.

To this end, we use both meteorological station data and reanalysis of the ERA5-Land data set from the C3S Climate Data Store (Copernicus Climate Change Service 2019).

2 Data and methods

CPE is situated along the Tyrrhenian Sea coast, covering 60 km^2, with a predominantly flat topography (for further details, refer to Nardone et al. 2025, this issue). The time series of meteorological data used for the climate analysis of CPE is sourced from three different origins: (1) the Castelporziano Presidential Estate Monitoring Network (CPE), (2) the Italian Air Force Meteorological Service (AM), and (3) the ERA5-Land gridded reanalysis (ERA5L).

Figure 1 illustrates the study area of CPE. In addition to the 12 weather stations of the CPE Monitoring Network (indicated by green circles within the CPE), two stations belonging to the Italian Air Force Meteorological Service are also highlighted (shown as blue circles). These stations, located in the vicinity of the CPE, are "Roma Fiumicino" to the north-west and "Pratica di Mare" to the south-east. Furthermore, the 15 ERA5-Land cell grids surrounding the

Fig. 1 Study area and location of meteorological datasets: CPE, AM, ERA5L (left panel); details of CPE meteorological monitoring network, indicating both historical (orange) and recent (green) stations (right panel). The shape file of CPE is retrieved from https://deims.org/0d2269d3-5423-4939-a30d-077c8bc38b03

study area are represented by red circles that indicate the center of each cell.

To analyze the climate patterns of the CPE, we gathered time series data on temperature and precipitation from 5 out of 12 weather stations of the CPE network. For the trend analysis, we used data from 3 out of 12 CPE stations in conjunction with two additional AM stations. The analysis also incorporated time series from 15 ERA5L grid cells. Furthermore, we compared the climate variability between CPE and its surrounding areas by utilizing a single grid point within the CPE (longitude E = 12.7, latitude N = 41.6) along with three grid points located in the urbanized sections of the city of Rome.

2.1 CPE meteorological stations

The CPE weather monitoring network has been operational since 1995, featuring both historical and more recent stations established in 2021 (Fig. 1). Currently, 12 weather stations are in operation, enabling real-time acquisition and analysis of environmental parameters (Table 1). The recorded meteorological measurements include air temperature (°C), relative humidity (%), precipitation (mm), soil temperature (°C), global solar radiation (W $^{m-2}$), and wind direction (°N) and speed (m s^{-1}). The weather stations used to collect the meteorological parameters consist of a shelter housing the data acquisition instruments, powered by a solar panel and a backup battery to ensure continuous data recording. The system is mounted on a 3-meter-high steel tripod equipped with sensors to measure air temperature, relative humidity, solar radiation, and wind direction and speed. In addition, the station includes an evaporation monitoring system composed of a rain gauge, a Class A evaporation Pan, an automatic sensor for measuring the water level in the pan. Soil temperature at a depth of 20 cm is also recorded. All instruments are connected to a data logger, with sensor measurements taken every 10 s, and the processed data are provided on an hourly and daily basis. For our analysis, we selected five stations that have at least one period of overlapping historical data. We then performed spatial interpolation for both temperature and precipitation using the Inverse Distance Weighting (IDW) method. Specifically, we utilized five stations with complete data records from 2015 to 2020 to construct climate patterns (Fig. 2).

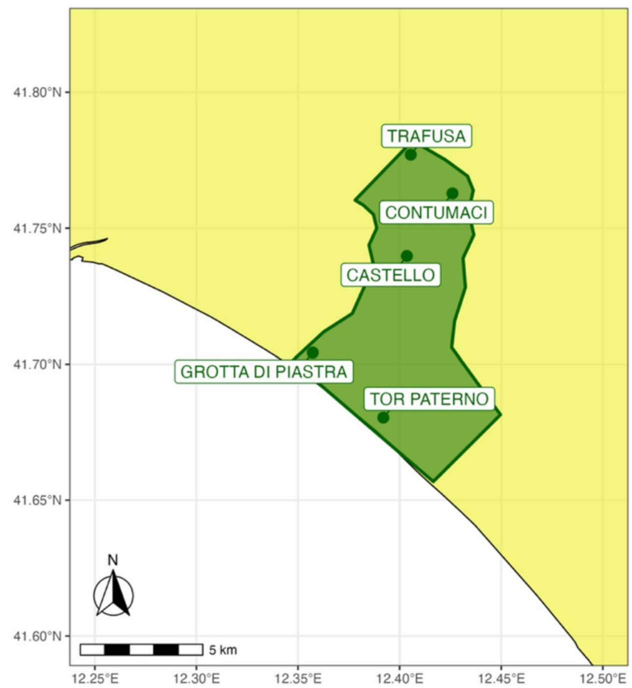

Fig. 2 Location of the meteorological stations used for building the climate patterns of the CPE

Table 1 CPE meteorological stations with relevant information

Name	ID	Coordinates	Description
Historical meteorological stations			
Castello	41-CPZ1	41°44′22.88″N 12°24′12.63″E	since 1995
Tor Paterno	42-CPZ2	41°40′49.37″N 12°23′31.12″E	since 1998
Campo Rota	43-CPZ4	41°43′37.84″N 12°23′33.17″E	since 2004
Trafusa	44-CPZ4	41°46′37.35″N 12°24′19.54″E	since 2008
Contumaci	46-CPZ6	41°45′46.03″N 12°25′33.60″E	since 2014
Grotte di Piastra	45-CPZ5	41°42′15.37″N 12°21′26.20″E	since 2012
Recent meteorological stations			
Santola	47-CPZ7	41°42′49.00″N 12°25′20.69″E	since 2021
Coltivati	48-CPZ8	41°43′46.12″N 12°25′05.00″E	since 2021
Antilopi	49-CPZ9	41°45′09.08″N 12°23′31.38″E	since 2021
Casal del Pastore	50-CPZ10	41°41′29.49″N 12°26′29.48″E	since 2021
Villa della Principessa	51-CPZ11	41°39′40.05″N 12°24′43.36″E	since 2021
Casal della dogana	52-CPZ12	41°42′08.15″N 12°23′44.29″E	since 2021

Furthermore, among the 5 weather stations of Fig. 2, we selected 3 weather stations that have a sufficiently long time series to allow for more in-depth climate analyses, such as trend and extreme event analysis: *Castello* with 29 years of data recorded, *Tor Paterno* with 25 years, and Trafusa with 16 years.

2.2 AM meteorological stations

The two stations of the Italian Air Force Meteorological Service network that were used are: *Roma Fiumicino* and *Pratica di Mare*. The former is located to the northwest of the CPE, the latter *Pratica di Mare* is located to the southeast. Both stations have a 44-year daily temperature and rainfall time series, from 1980 to 2023.

2.3 ERA5-land

Climate reanalysis integrates model data with global observations to create a complete and consistent dataset using the laws of physics. This method allows for data dating back several decades, providing an accurate representation of past climate conditions. For instance, ERA5-Land describes the evolution of the water and energy cycles over land in a consistent manner, which can be useful for analyzing trends and anomalies (Muñoz-Sabater et al. 2021). ERA5-Land retains most of the parameterizations found in ERA5 but features a higher horizontal resolution, achieving a global resolution of 9 km compared to ERA5's 31 km. Both datasets have an hourly temporal resolution, and the time series runs from 1950 to the present. Climate data from ERA5-Land are provided as a raster of hourly data in a uniform grid, with each grid cell measuring $0.1° \times 0.1°$. The Coordinate Reference System (CRS) used is WGS84. Hourly data for temperature and precipitation were downloaded in GRIB format and then aggregated to daily resolution. This resulted in a time series covering January 1950 to December 2023. Additionally, temperature data were converted from Kelvin to Celsius using the equation $T(°\mathrm{C}) = T(\mathrm{K}) - 273.15$. Precipitation data were transformed from meters to millimetres. The daily time series for temperature and precipitation from ERA5-Land were analyzed in *R* using the terra library (Hijmans 2023).

2.4 Outliers detection and data imputation

In statistics, the term imputation is used to mean the replacing of missing data in a time series. Two general approaches for imputing multivariate data have emerged recently: (1) joint modeling (JM) and (2) fully conditional specification (FCS), also known as multivariate imputation by chained equations (MICE). Schafer (1997) developed various JM techniques for imputation under the multivariate normal, the log-linear, and the general location model. JM involves specifying a multivariate distribution for the missing data and drawing imputation from their conditional distributions using Markov chain Monte Carlo (MCMC) techniques.

In contrast, FCS specifies the imputation model on a variable-by-variable basis through a set of conditional densities, one for each incomplete variable (van Buuren 2007). FCS begins with an initial imputation and iteratively draws new imputations based on these conditional densities. Typically, a low number of iterations (around 10–20) is sufficient for this process to reach a satisfactory quality of replacing, one for each incomplete variable (van Buuren 2007).

Before applying the FCS imputation model, we checked the entire set of time series to identify any outliers and anomalies in the data, categorizing these as missing data. For this purpose, we utilized standard methods such as the Tukey boxplot (Tukey 1949) and the Hampel filter (Hampel 1974).

Initially, we filled in the missing data in the AM time series by taking into account temperature and precipitation data from both the *Roma Fiumicino* and *Pratica di Mare* stations. Following this, we used the filled AM time series data along with the five selected CPE stations to impute missing values in their datasets. This multivariate approach ensures the comprehensive use of all available data.

As an example, we present in Fig. 3 the alternatives for replacing daily time series data of maximum temperature and precipitation at *Castello*. In this figure, the blue points represent the existing data and are consistent across the different panels, while the red points vary, representing the potential replacement data. The red points generally follow a similar pattern to the blue points, indicating they are plausible measurements. Furthermore, the variation among the red points illustrates our uncertainty regarding the true (but unknown) values.

In this study, we used the FCS multiple imputation approach and the mice R package (van Buuren and Groothuis-Oudshoorn 2011) to fill missing data.

2.5 Trend test

To test the presence of a trend in a time series, it is possible to use either a parametric or a nonparametric statistical test. The parametric is always more powerful than a nonparametric test; furthermore, the null hypothesis H0 of a parametric is a more explicit statement about the presence or absence of a linear trend than a nonparametric approach. Say β the trend coefficient, the null hypothesis H0 for a parametric approach is that $\beta = 0$. In contrast, a nonparametric test evaluates evidence counter to the statement: the data are a sample of n independent and identically distributed (iid) random variables. In the latter case, H0 is false when $\beta = 0$. In this study, we use the Mann-Kendall trend test, which belongs to the family of nonparametric tests.

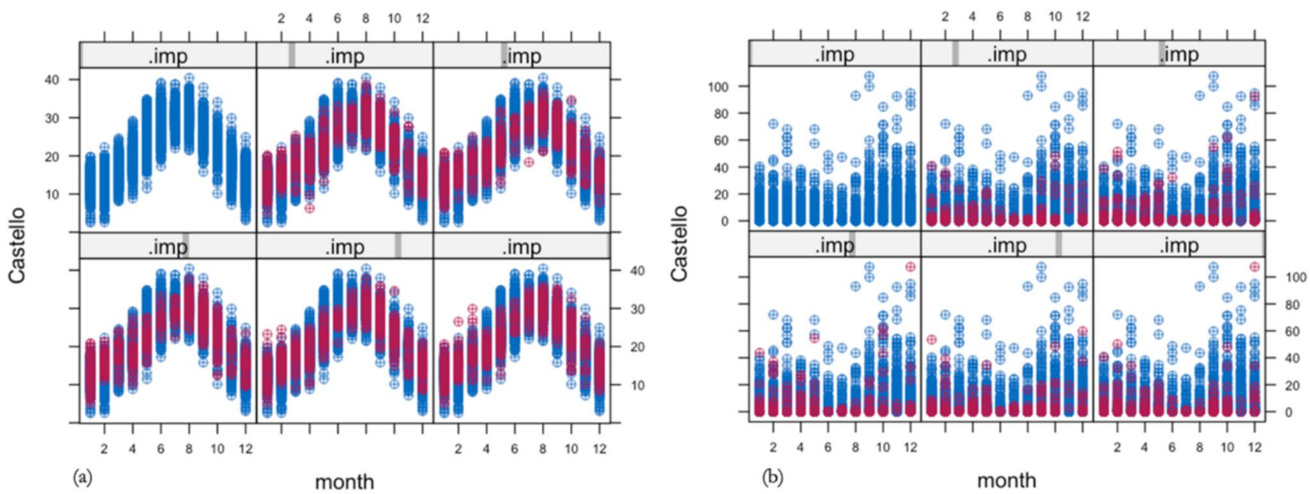

Fig. 3 Replaced missing data in Castello daily time series (**a**) maximum temperature, (**b**) precipitation

Furthermore, we use the β-Sen methodology to compute the magnitude of trend (Sen 1968). In practice, trend magnitude is the median of slopes obtained from all the possible combinations of two points in the time series. To this end, the R package zyp was used Bronaugh and Schoeneberg (2023). Climate time series, especially on a daily scale, might be influenced by autocorrelation. Since a positive autocorrelation in the time series leads the test to reject the null hypothesis more often (von Storch 1999), we applied the approach proposed by Zhang et al. (2000) to correct the time series before application of trend test. This iterative method starts from a first computation of autocorrelation to obtain a de-correlated series by applying the autoregressive (AR) method of order 1. Then, the β-Sen coefficient is calculated from the de-correlated series, which, in turn, is used to de-trend the historical series. The algorithm proceeds following this scheme until the parameter estimates are stable. The Mann-Kendall trend test corrected for autocorrelation was applied over the entire time series of temperature and precipitation, as well as over the climate extreme indices described in Sections 2.3 and 2.4. A more detailed description of the full procedure is provided in Di Giuseppe et al. (2019).

2.6 Standardized precipitation-evapotranspiration index

The Standardized Precipitation Evapotranspiration Index (SPEI) represents a basic climate water balance, combining precipitation and potential evapotranspiration (PET) to describe simplified temperature–precipitation dynamics, especially under climate change conditions. The SPEI concept was developed by Vicente-Serrano et al. (2009). It is calculated based on the monthly (or longer) difference between precipitation and Potential Evapotranspiration (PET).

More specifically, the long-term time series of this difference is fitted to a log-logistic distribution to estimate parameters that transform the data into a standard normal variable with a mean of zero and a variance of one. As a result, the SPEI follows a Gaussian distribution, where the magnitude of deviation from the mean serves as a probabilistic measure of the severity of wet or dry events. The temporal scale of aggregation—be it quarterly, 6-monthly, 12-monthly, or 24-monthly—represents different types of drought features, namely meteorological, agronomic, hydrological, and socio-economic, respectively. Even if it is just a climate-driven water balance proxy, SPEI accounts for temperature-driven evapotranspiration, making it more sensitive to warming trends linked to the climate crisis.

PET is considered a proxy for the atmospheric demand for water, indicating the amount of evaporation and transpiration that would occur if a sufficient water source were available. We calculated PET using the Hargreaves equation, as described by Hargreaves (1994). This equation computes the monthly reference evapotranspiration (ET0) for a grass crop by utilizing the mean external radiation, which is estimated based on latitude and the month of the year. Since SPEI approximates climatic demand vs. supply, it is not suitable to represent the full complex interaction dynamic of heatwaves and drought periods, but it enables us to analyze trends for such a simplified water balance, highlighting robust long-term climatic regimes and phases in a changing climate. The SPEI package in R was employed to compute both PET and SPEI (Beguería and Vicente-Serrano 2023).

The data was accumulated to create a SPEI time series with a 12-month resolution, covering the available period for each time series.

2.7 Climate change indices

To establish a common methodology for evaluating variations in climate extremes and to ensure comparability of results across different regions, the Expert Team on Climate Change Detection and Indices (ETCCDI), part of the CLIVAR Working Group on Climate Change Detection under the Commission for Climatology of the World Meteorological Organization (WMO), has developed a set of 27 indices. These indices effectively describe temperature and precipitation extremes in terms of frequency, intensity, and duration.

For the analysis of climate extremes in the CPE, we identified 4 temperature indices (Table 2) and 9 precipitation indices (Table 3) from those recommended by the ETCCDI. These indices are relevant and significant for the typical climate at these latitudes, as they describe extreme events. The indices are calculated on both a seasonal and an annual basis. To this end, we used the *ClimInd* R package (Reig-Gracia et al. 2021).

3 Results

3.1 Temperature and precipitation patterns

To examine the spatial variation of temperature and precipitation in the CPE, data recorded by 5 out of 12 stations in the CPE monitoring network were selected for the period from 2015 to 2020 (Fig. 2). Using the seasonal averages, or cumulative data in the case of precipitation, an Inverse Distance Weighted (IDW) spatial interpolation method was applied. This method was used to create maps illustrating the spatial patterns of maximum temperature (Fig. 4), minimum temperature (Fig. 5), and precipitation (Fig. 6).

The CPE, like other areas of the Lazio coastline, experiences climatic variability influenced by both its proximity to the Tyrrhenian Sea and the increasing distance from the coast towards the inland areas. This geographical transition affects seasonal temperatures and precipitation, creating climatic differences between coastal and inland areas.

Analyzing the temperature maps, particularly the seasonal maximum temperatures, shows a thermal gradient that extends from the coastline to the interior of the CPE. During the hottest season (June, July, August, JJA), the average seasonal maximum temperature is lowest at the coastline, measuring around 28 °C, while in the interior, temperatures can reach or even exceed 31 °C. Winter along the coast is generally mild, with average temperatures around 9–10 °C in January. In the inland areas, temperatures can drop further, especially during nighttime. During spring, temperatures along the coast are mild, with average values gradually increasing from March to May. Moving inland, daytime temperatures can be slightly higher, but daily temperature variations tend to increase, as shown by the pattern of minimum temperatures. Summer along the coast is characterized by high temperatures, which are largely mitigated by the marine influence. Coastal average temperatures in July and August are around 24–25 °C. Inland, temperatures are higher, frequently exceeding 30 °C during the day, with warmer nights due to the urban heat island effect, which is visible on maps both in the inland areas of the CPE and along its northwestern edge. Autumn temperatures gradually decrease. The

Table 2 Summary of ETCDDI climate indices for the temperature

Index	Definition	Units
TXx	Maximum of daily maximum temperature in a given period	°C
SU	Number of days where TX > 25 °C	days
WSDI-TX	Number of at least six consecutive days where TX > 90th percentile	days
WSDI-TN	Number of at least six consecutive days where TN > 90th percentile	days
TR	Number of days where TN > 20 °C	days

Table 3 Summary of ETCDDI climate indices for the precipitation

Index	Definition	Units
RX1day	Maximum of 1-day precipitation	mm
RX5day	Maximum of consecutive 5-day precipitation	mm
SDII	Annual total precipitation by the number of wet days	mm/days
R10	Number of days when precipitation ≥ 10 mm	days
R20	Number of days when precipitation ≥ 20 mm	days
R95pTOT	Precipitation at days exceeding the 95th percentile by total precipitation	%
R99pTOT	Precipitation at days exceeding the 99th percentile by total precipitation	%
CDD	Maximum number of consecutive days with precipitation < 1 mm	days
CWD	Maximum number of consecutive days with precipitation ≥ 1 mm	days

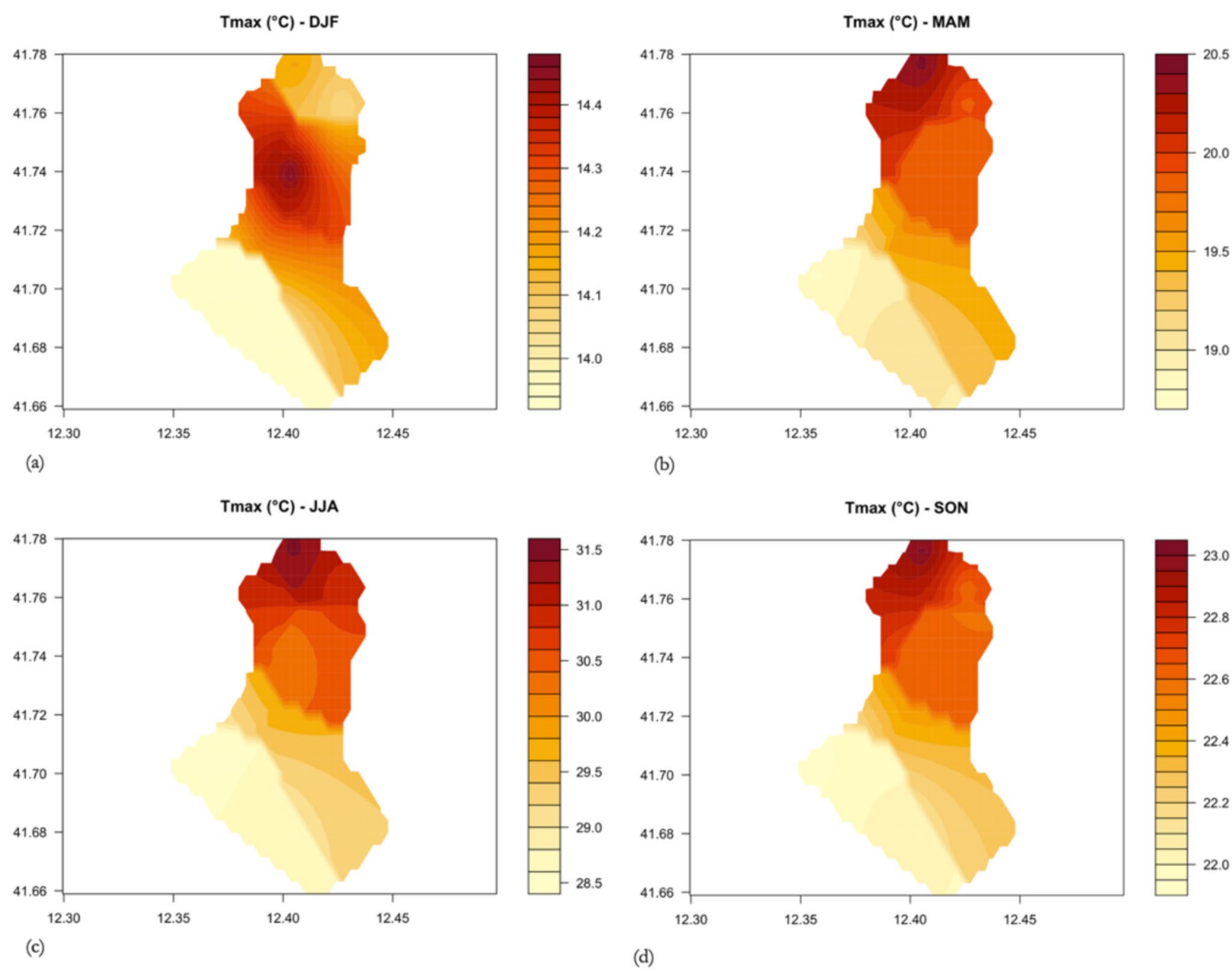

Fig. 4 Seasonal patterns of maximum temperature (IDW, 2015–2020): DJF (**a**), MAM (**b**), JJA (**c**), SON (**d**)

coast benefits from the sea's thermoregulatory effect, keeping temperatures milder compared to inland areas.

Winter precipitation is frequent and substantial. Inland areas tend to record higher accumulations than the coast. Spring precipitation is generally moderate. During this period as well, inland areas can experience slightly higher accumulations compared to the coast, due to greater atmospheric instability over land compared to the coastline. Summer is naturally the driest season. Precipitation is scarce both along the coast and inland, with occasional summer thunderstorms more likely in the inland areas, again due to greater atmospheric instability. Autumn is the wettest season. Precipitation increases significantly, with higher accumulations in inland areas compared to the coastal zone.

By analyzing the longest available time series from the CPE monitoring network stations, we focused on three specific stations that effectively represent the spatial diversity of the CPE. These stations are *Tor Paterno*, located on the coast; *Castello*, situated in the central area of the reserve; and *Trafusa*, which is located in the innermost section and is closest to the neighboring urban area (Fig. 2 in Sect. 2).

The time series data for annual maximum temperature (Fig. 7a) and annual minimum temperature (Fig. 7b) indicate a clear thermal gradient from the coastline toward the interior, as shown in the climate patterns of Figs. 4 and 5. Specifically, the average maximum temperature at *Tor Paterno* (located on the coast) is approximately 2 °C lower than that at *Trafusa* (situated in the innermost part), while the minimum temperature at *Tor Paterno* is about 3 °C lower than at *Trafusa*. Additionally, although the historical data series is not equally long for all three locations, there is a noticeable general warming trend in recent years.

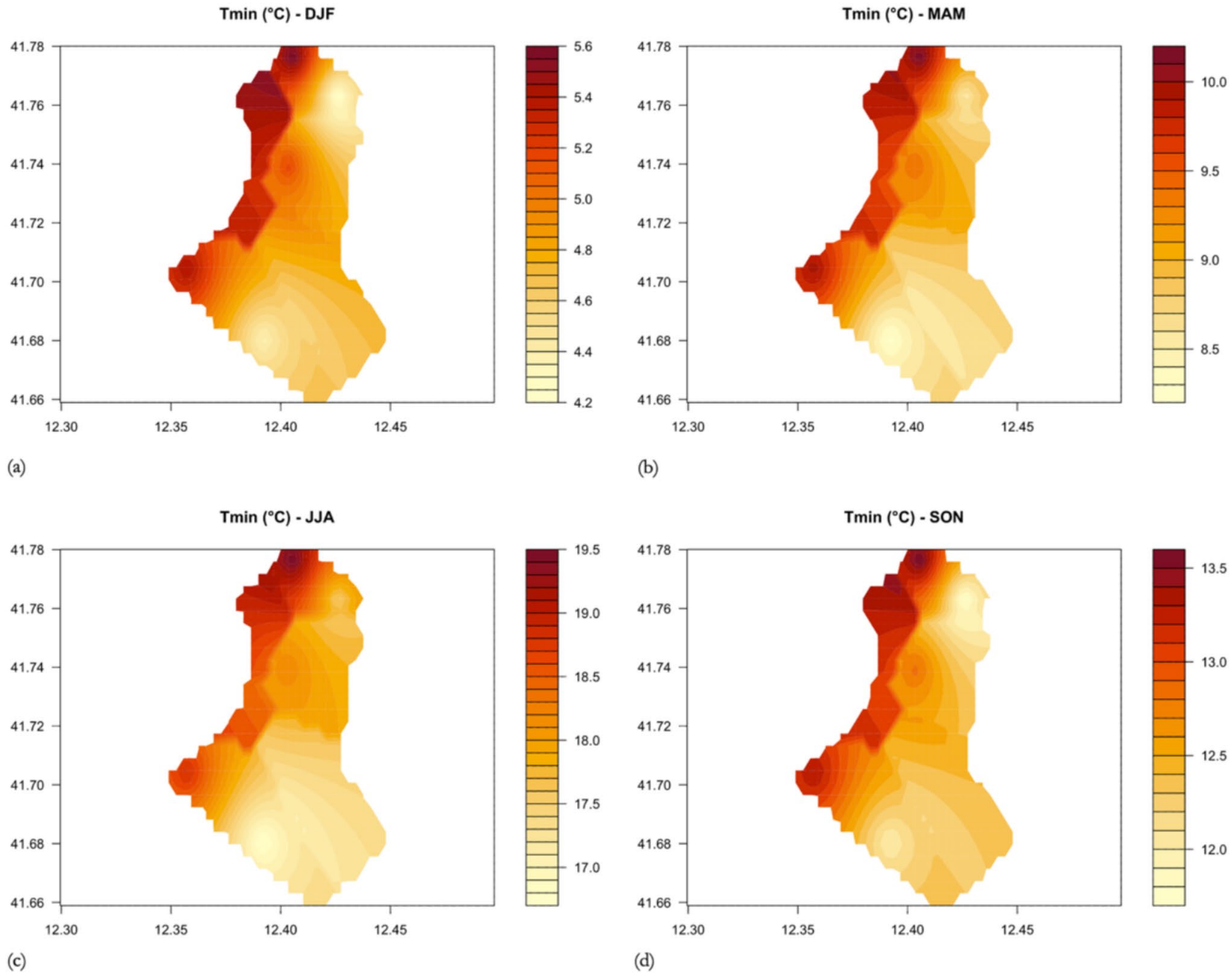

Fig. 5 Seasonal patterns of minimum temperature (IDW, 2015–2020): DJF (**a**), MAM (**b**), JJA (**c**), SON (**d**)

3.2 Trend analysis of temperature

To improve the insights gained from the time series visualization of Fig. 7, a trend analysis of temperature data was conducted for *Castello* and *Tor Paterno*. Unlike *Trafusa*, these two locations provided a sufficiently long observation period of 29 years, spanning from 1995 to 2023. Additionally, the time series data from the two AM weather stations, *Roma Fiumicino* and *Pratica di Mare*, were analyzed to provide a benchmark for comparison with surrounding areas. To achieve this, the timeframe for the AM time series was set from 1995 to 2023. The trend results are presented in Table 4 for maximum, minimum, and diurnal averaged temperatures. Following standard practices, a *P*-value of 0.05 or less indicates a statistically significant trend. Additionally, two columns are provided to report the following: (a) the estimated variation per year, along with the corresponding confidence interval (denoted as *β-sen*); and (b) the total variation that occurred during the period from 1995 to 2023 (Trend).

Overall, it seems that the warming trend for maximum temperatures (T_{max}) occurs more often than for minimum temperatures (T_{min}), while for diurnal temperatures (T_{avg}), it appears that yearly and seasonal trends are more similar to those of T_{max} than T_{min}. Specifically, when looking at yearly data, the increasing trend in T_{max} is consistent across the four locations, with values ranging from +1.2 to +1.5 °C. In contrast, the trend for T_{min} is not statistically significant.

However, at a seasonal level, there is a notable warming trend for T_{min} during winter, with increases of +1.7 °C at *Castello* and +1.5 °C at *Tor Paterno*. There is no significant trend for T_{max} during this season. In summer and autumn, the warming trend for temperatures reaches its highest levels, with increases up to +3.2 °C.

The trend analysis was completed by computing the test trend for each time series of ERA5L cell grids. The trend

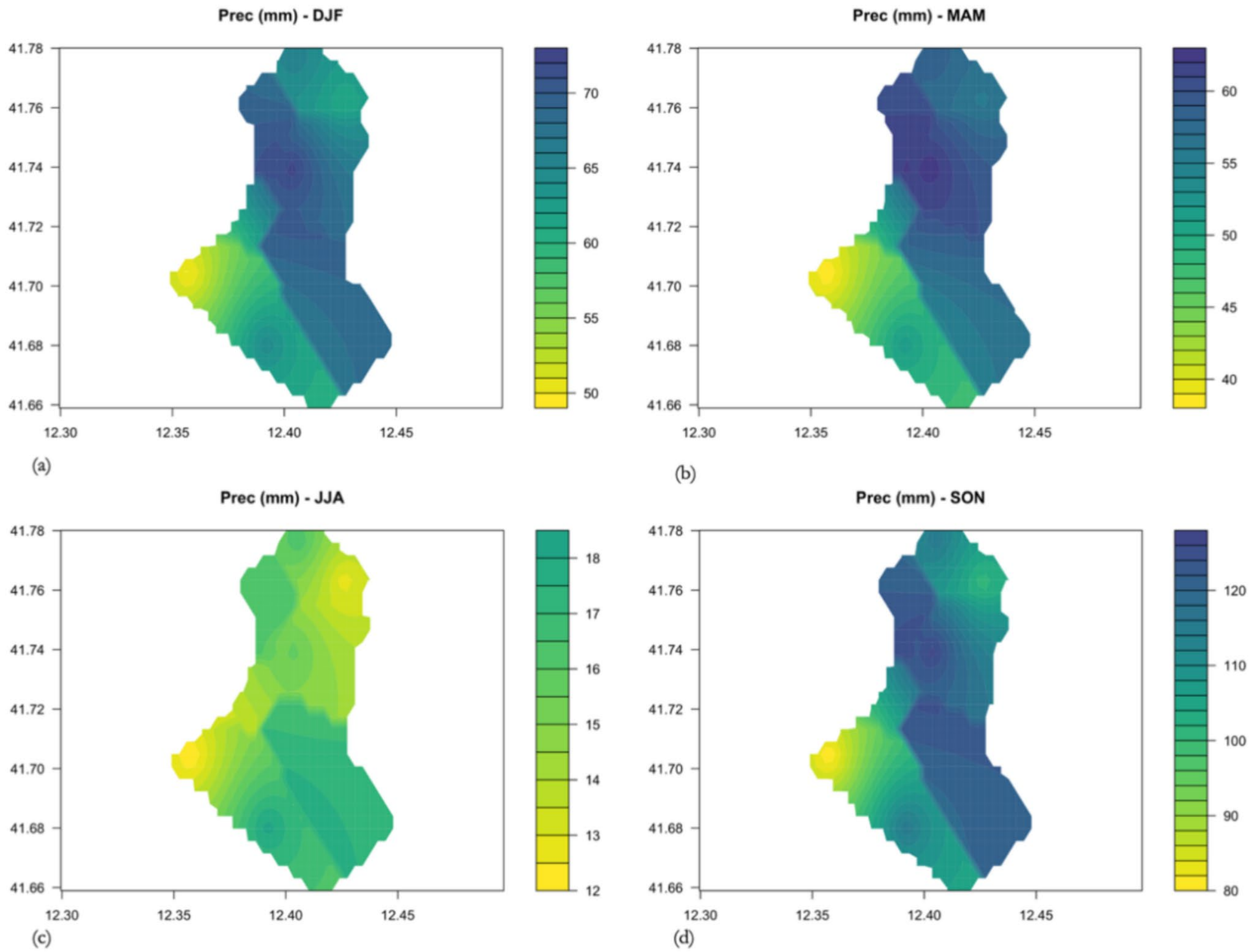

Fig. 6 Seasonal patterns of precipitation (IDW, 2015–2020): DJF (**a**), MAM (**b**), JJA (**c**), SON (**d**)

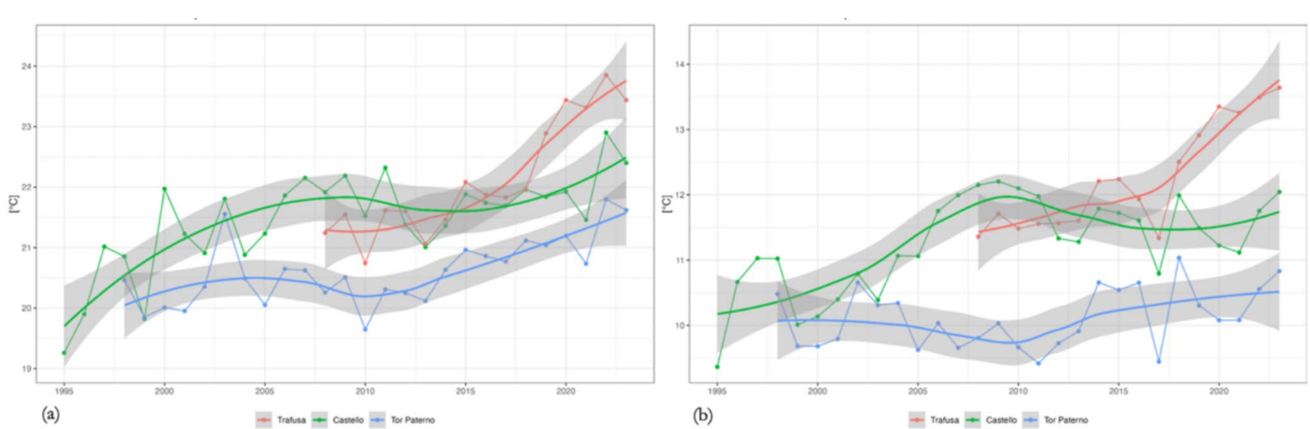

Fig. 7 Annual time series of temperature for Trafusa, Castello, and Tor Paterno weather stations: (**a**) average maximum temperature, (**b**) average minimum temperature

Table 4 Trend of annual and seasonal maximum (T_{max}), minimum (T_{min}), and diurnal temperature (T_{avg}) time series from Castello, Tor Paterno, Pratica di Mare, and Roma Fiumicino meteorological stations in the time window 1995–2023 (29 years), except Tor Paterno (1999–2023). β-sen is the quote of yearly variation in °C along with the lower and upper bounds of the confidence estimates. The "Trend (°C)" column indicates the total temperature variation in °C from the beginning to the end of the analysed period. A P-value of ≤0.05 indicates a strong level of confidence in the trend estimate; values greater than 0.05 are considered not statistically significant and indicated as "n.s."

Location	Period	Maximum temperature (T_{max})				Minimum temperature (T_{min})				Diurnal temperature (T_{avg})			
		β-sen (°C)		P-value	Trend (°C)	β-sen (°C)		P-value	Trend (°C)	β-sen (°C)		P-value	Trend (°C)
Castello	YEAR	0.051	(0.014–0.082)	0.005	+1.5	–	–	0.243	n.s	0.038	(0.008–0.072)	0.019	+1.1
Tor Paterno	YEAR	0.059	(0.029–0.082)	0.001	+1.5	–	–	0.052	n.s	0.723	(0.008–0.008)	0.008	+1.1
Pratica Di Mare	YEAR	0.041	(0.016–0.071)	0.007	+1.2	–	–	0.514	n.s	–	–	0.138	n.s
Roma Fiumicino	YEAR	0.051	(0.031–0.069)	0.001	+1.5	–	–	0.652	n.s	0.026	(0.0–0.05)	0.046	+0.8
Castello	DJF	–	–	0.770	n.s	0.017	(0.009–0.096)	0.017	+1.7	–	–	0.133	n.s
Tor Paterno	DJF	–	–	0.784	n.s	0.039	(0.009–0.117)	0.039	+1.5	–	–	0.061	n.s
Pratica Di Mare	DJF	–	–	0.373	n.s	–	–	0.333	n.s	–	–	0.797	n.s
Roma Fiumicino	DJF	–	–	0.138	n.s	–	–	0.118	n.s	–	–	0.952	n.s
Castello	MAM	–	–	0.566	n.s	–	–	0.890	n.s	–	–	0.514	n.s
Tor Paterno	MAM	–	–	0.262	n.s	–	–	0.743	n.s	–	–	0.468	n.s
Pratica Di Mare	MAM	–	–	0.778	n.s	–	–	0.260	n.s	–	–	0.514	n.s
Roma Fiumicino	MAM	–	–	0.277	n.s	–	–	0.489	n.s	–	–	0.858	n.s
Castello	JJA	0.088	(0.043–0.135)	0.001	+2.5	0.006	(0.014–0.116)	0.006	+1.9	0.075	(0.044–0.107)	0.001	+2.2
Tor Paterno	JJA	0.071	(0.033–0.116)	0.007	+1.9	0.021	(0.018–0.132)	0.021	+2.1	0.072	(0.025–0.108)	0.008	+1.9
Pratica Di Mare	JJA	0.072	(0.008–0.155)	0.025	+2.1	0.025	(0.009–0.159)	0.025	+2.5	0.068	(0.001–0.135)	0.046	+2.0
Roma Fiumicino	JJA	0.111	(0.070–0.155)	0.001	+3.2	0.0002	(0.040–0.110)	0.0002	+2.2	0.094	(0.049–0.131)	0.00003	+2.6
Castello	SON	0.065	(0.020–0.112)	0.003	+1.9	0.006	(0.022–0.094)	0.006	+1.7	0.069	(0.031–0.097)	0.004	+2.0
Tor Paterno	SON	0.052	(0.013–0.099)	0.009	+1.3	–	–	0.088	n.s	0.052	(0.007–0.092)	0.026	+1.4
Pratica Di Mare	SON	0.077	(0.029–0.115)	0.002	+2.2	0.046	(0.004–0.165)	0.046	+3.1	0.089	(0.017–0.139)	0.010	+2.6
Roma Fiumicino	SON	0.061	(0.036–0.092)	0.001	+1.8	–	–	0.499	n.s	0.038	(0.007–0.073)	0.019	+0.8

analysis was conducted by calculating the trend for each time series derived from the ERA5L cell grids.

To support our findings, we previously examined the correlation between the ERA Land dataset and observational data. Specifically, we extracted the time series from individual cell grids that overlap with the CPE area and calculated the Pearson correlation coefficients for the time series related to the CPE monitoring network, including the data from *Castello* and *Tor Paterno*. Additionally, we analyzed the data from *Pratica di Mare* for the AM monitoring network, which is located in the same cell grid. The results of the statistical tests conducted to evaluate the significance of the correlations indicate that, with very few exceptions, there is a strong correlation at both the yearly and seasonal scales, which are relevant for this analysis (Table 5). Although there is no evidence of a trend in precipitation, we observe a strong correlation between the ERA5 Land data and the observed precipitation time series.

Coloured maps indicating various levels of trend variation are obtained both for annual and seasonal aggregation. Figures 8 and 9 illustrate the variation in annual and seasonal maximum and minimum temperatures over a 29-year period (1995–2023) using the ERA5L as well as the observational dataset, both within the CPE and its neighboring regions.

Table 5 Pearson's correlation coefficients calculated between the ERA5 Land time series and those of Castello and Tor Paterno for the CPE monitoring network, as well as Pratica di Mare for the AM monitoring network

Location	Period	Correlation ERA5L-observations		
		Maximum temperature (T_{max})	Minimum temperature (T_{min})	Total precipitation (Prec)
Castello	YEAR	0.66***	0.31 n.s	0.81***
Tor Paterno	YEAR	0.85***	0.64***	0.77***
Pratica Di Mare	YEAR	0.65***	0.60***	0.41**
Castello	DJF	0.87***	0.73***	0.63***
Tor Paterno	DJF	0.96***	0.87***	0.88***
Pratica Di Mare	DJF	0.87***	0.78***	0.76***
Castello	MAM	0.80***	0.43**	0.87***
Tor Paterno	MAM	0.83***	0.72***	0.90***
Pratica Di Mare	MAM	0.47**	0.67***	0.82***
Castello	JJA	0.79***	0.61***	0.76***
Tor Paterno	JJA	0.92***	0.88***	0.89***
Pratica Di Mare	JJA	0.84***	0.76***	0.68***
Castello	SON	0.82***	0.67***	0.59***
Tor Paterno	SON	0.93***	0.87***	0.60***
Pratica Di Mare	SON	0.80***	0.86***	0.17 n.s

***P value < 0.05; **P value < 0.10; values greater than 0.05 are considered not statistically significant and indicated as "n.s."

It is crucial to note that trend values for each grid cell and for the weather station points are statistically significant at the 0.05 level, unless stated otherwise as "not statistically significant".

Regarding the annual aggregation, in the case of T_{max}, there is a notable increase in temperature variation, particularly in the innermost and urbanized areas of the region, where values range from +1.6 °C to +1.8 °C. Closer to the coastline, the trends show an upward pattern as well, with values between +1.0 °C and +1.4 °C.

In contrast, for T_{min}, there is no evidence of differing trend variations between CPE and the surrounding areas. However, the warming within the CPE is slightly higher than that observed for T_{max}, ranging from +1.4 °C to +1.6 °C compared to +1.2 °C to +1.4 °C for T_{max}.

It is important to note that, in the case of T_{max}, the trend values reported for the two stations in the CPE monitoring network and the two AM stations, as detailed in Table 4, are consistent with those of the ERA5L dataset. Specifically, the *Castello*, *Tor Paterno*, and *Rome Fiumicino* stations recorded a positive trend of approximately +1.5 °C, while the *Pratica di Mare* station reported a trend of about +1.2 °C. Conversely, for T_{min}, there is no statistical evidence of a trend at the weather station locations; however, a strong trend is evident in the ERA5L spatially interpolated dataset.

The trend maps of seasonal maximum temperatures illustrate a positive gradient from the coastline toward the interior during summer (JJA) and autumn (SON). In contrast, in winter (DJF) and spring (MAM), there is no evidence of a significant trend. The trend variation of the CPE that results from ERA5L ranges from +1.4 to +1.8 °C in summer and from +1.6 to +1.8 °C in autumn. The examined weather stations align with the ERA5L dataset, with summer trends of +2.1 °C at *Pratica di Mare*, +3.2 °C at *Rome Fiumicino* for AM stations, and +2.5 °C at *Castello* and +1.8 °C at *Tor Paterno* for the CP network. For autumn, the values are +2.2 °C at *Pratica di Mare*, +1.8 °C at *Rome Fiumicino*, +1.9 °C at *Castello*, and +1.3 °C at *Tor Paterno*.

Again, at the seasonal scale, the minimum temperature does not show any trend for the winter (DJF) and spring seasons (MAM). However, *Castello* and *Tor Paterno* result in a trend of +1.7 °C and +1.5 °C, respectively. In the summer (JJA) and autumn (SON) seasons, the trend estimated from ERA5L is between +1.8 °C and +2.0 °C, a variation which aligns with the results of weather stations: in Summer (JJA), it exceeds +2.0 °C at the *Tor Paterno*, *Pratica di Mare*, and *Rome Fiumicino*, and is equal to +1.9 °C at *Castello*; in Autumn (SON), the variation is +1.7 °C at *Castello* and exceeds +3.0 °C at *Pratica di Mare*, while there is no evidence of trend at *Tor Paterno* and *Rome Fiumicino*.

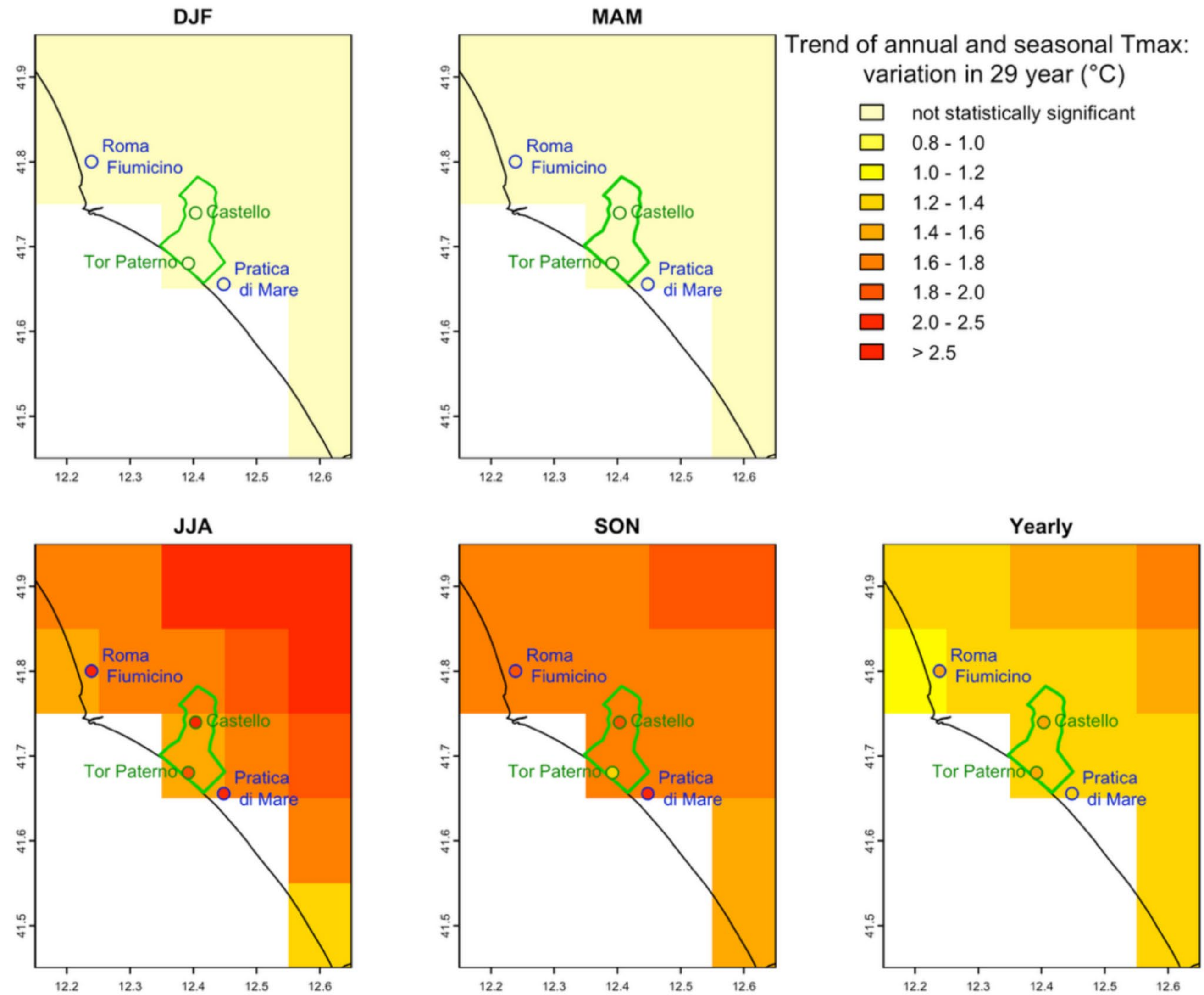

Fig. 8 Trend variation of yearly and seasonal maximum temperatures calculated using both the ERA5 Land and observational datasets. Green circles represent CPE weather stations, while blue circles indicate the AM network stations. Trend values are displayed in color-coded classes for each grid cell and for the weather station points. All reported trends are statistically significant at the 0.05 level, unless stated otherwise as "not statistically significant," which is indicated by light yellow

Finally, the trend analysis of precipitation, both in the case of ERA5L and weather station data (not shown), reveals that there is no statistically significant trend either in the CPE or surrounding areas.

3.3 Comparing temperature conditions of CPE and surrounding urban areas

To determine whether there is a difference in climate between the CPE and the surrounding urbanized territory, specifically the city of Rome, the anomaly of maximum temperature using ERA5L data was analyzed. The period from 1981 to 2010 is used as a reference for normal climate conditions (Cli.no.). Then, the difference between the yearly maximum temperature (T_{max}) and the normal climate conditions was calculated for the time frame from 1951 to 2023. As illustrated in Fig. 10, progressive warming is clearly evident in all seasons for both the CPE and the urbanized area of Rome. However, during the summer months (JJA), particularly in recent years, the positive thermal anomaly in the urbanized area of Rome is significantly higher than that in the CPE. In the same season, there is also a strong mark of colder years in the urbanized area of Rome compared to CPE during the '70s.

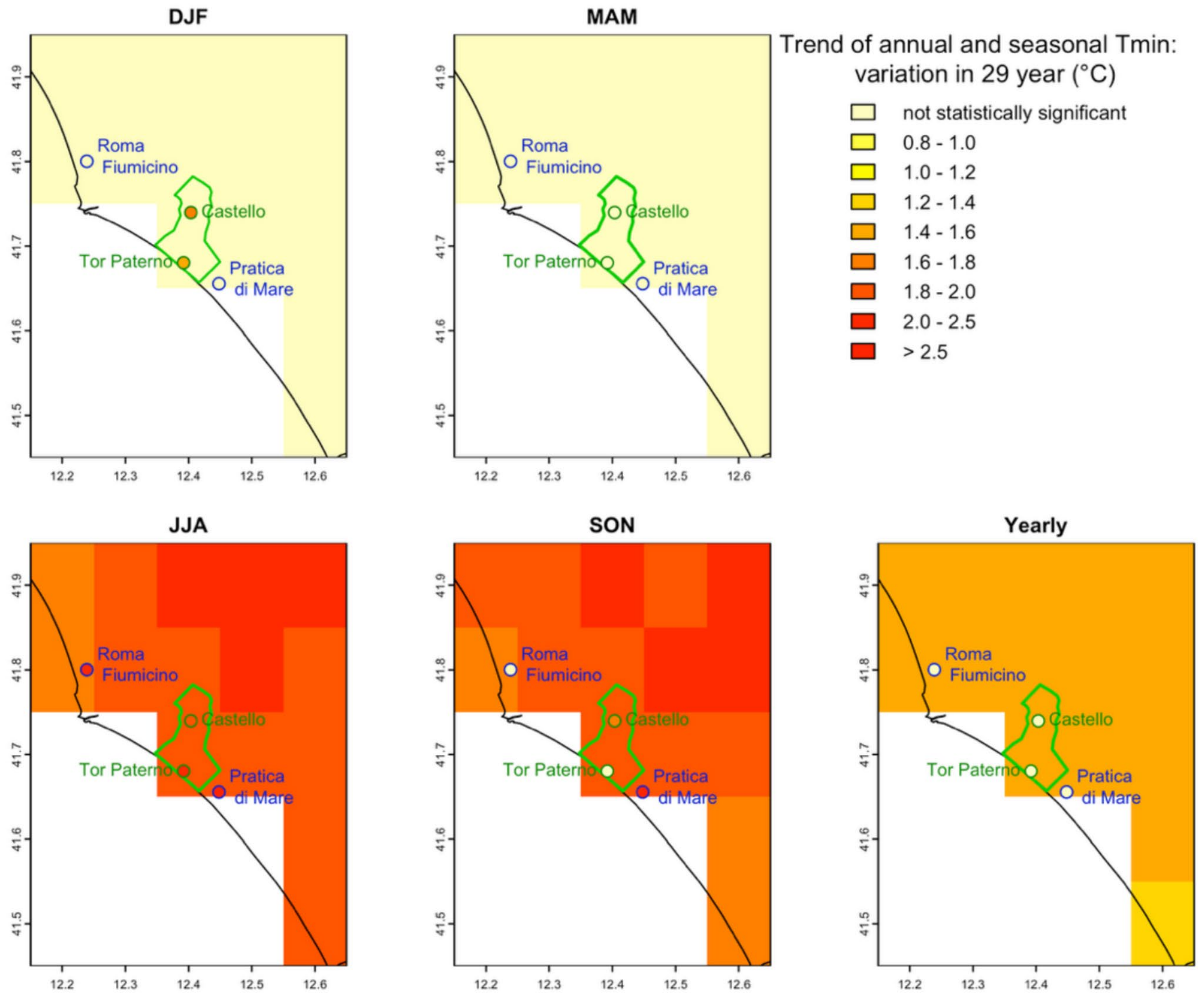

Fig. 9 Trend variation of yearly and seasonal minimum temperatures calculated using both the ERA5 Land and observational datasets. Green circles represent CPE weather stations, while blue circles indicate the AM network stations. Trend values are displayed in color-coded classes for each grid cell and for the weather station points. All reported trends are statistically significant at the 0.05 level, unless stated otherwise as "not statistically significant," which is indicated by light yellow

3.4 Temperature and precipitation joint analysis

To have a better overview of the combined deviations from normal conditions of temperature and precipitation, both anomalies in a single graph was depicted. In this way, it is easier to answer the question of whether a particular year was dry-warm or wet-cold and even compare these anomalies in the context of previous years. In Fig. 11 the last 10 years (from 2014 to 2023) of the series are marked in green and it is quite evident how, for all three stations, they are almost all located in the hot-dry and hot-humid sectors, attesting once again to the warming tendency emerged through the trend analysis.

The Standardized Precipitation-Evapotranspiration Index (SPEI) measures the combined effects of precipitation and temperature. In this study, a temporal scale of 12 months is used, meaning that each monthly SPEI value reflects the aggregated conditions from the preceding 12 months. Additionally, due to the standardization process used to calculate the index, a SPEI value of −1 is typically used to indicate drought events. Figure 12 displays the time series of SPEI12 for the CPE weather stations of *Trafusa*, *Castello*, and *Tor Paterno*.

The time series reveals several episodes of drought at *Castello*: two episodes occurred from 2000 to 2003, a shorter event took place in 2004 (during winter) and 2005 (during

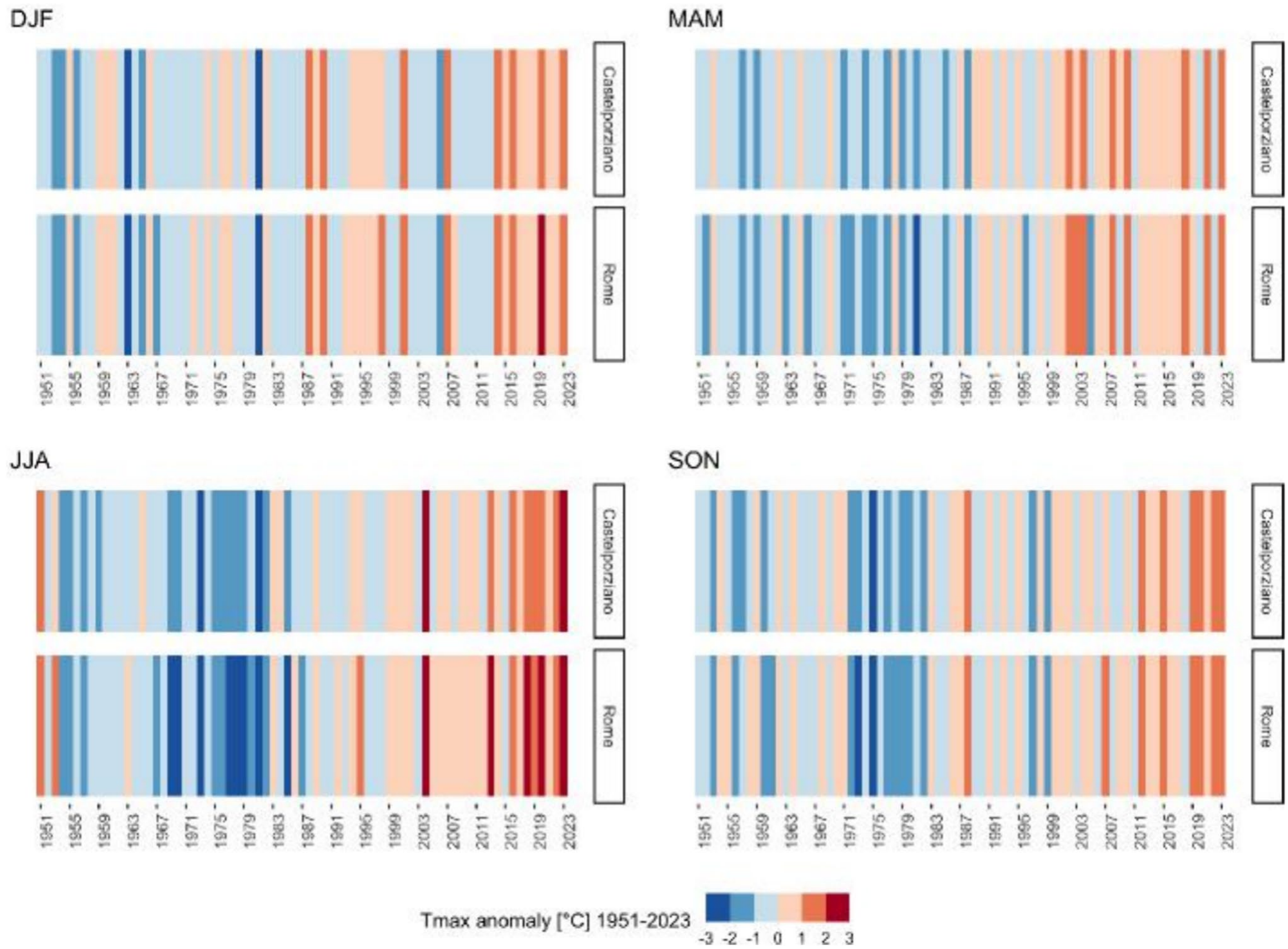

Fig. 10 Warming stripes of T_{max} anomaly with respect to normal conditions

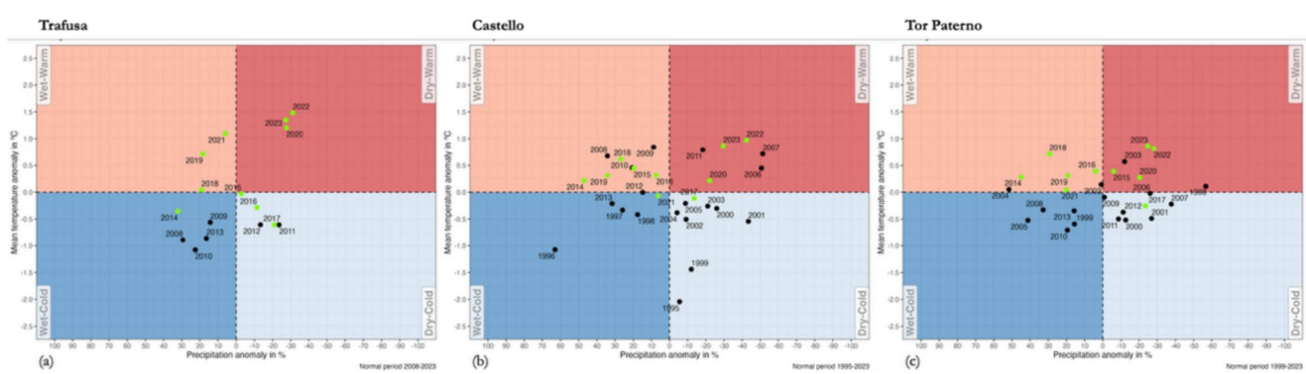

Fig. 11 Combined anomalies of temperature and precipitation for the CPE meteorological stations of (**a**) Trafusa, (**b**) Castello, and (**c**) Tor Paterno. Notice that yearly anomalies of precipitation are in percentage, and the x-axis is in the reverse order from the most humid to the driest

summer), a prolonged episode lasted from 2007 to 2008, and another similar event was recorded from 2022 through 2023. The drought episodes recorded at the *Tor Paterno* station on the coast include those from 2002 to 2003, 2007 to 2008, and 2022 to 2023. In contrast to the findings from the *Castello* station, 2005 experienced an abundance of available water. Additionally, there are drought episodes noted at *Tor Paterno* that were not observed at *Castello*: in 2012 (during summer), 2016 (summer and part of autumn), and 2017–2018 (summer, autumn, and part of winter).

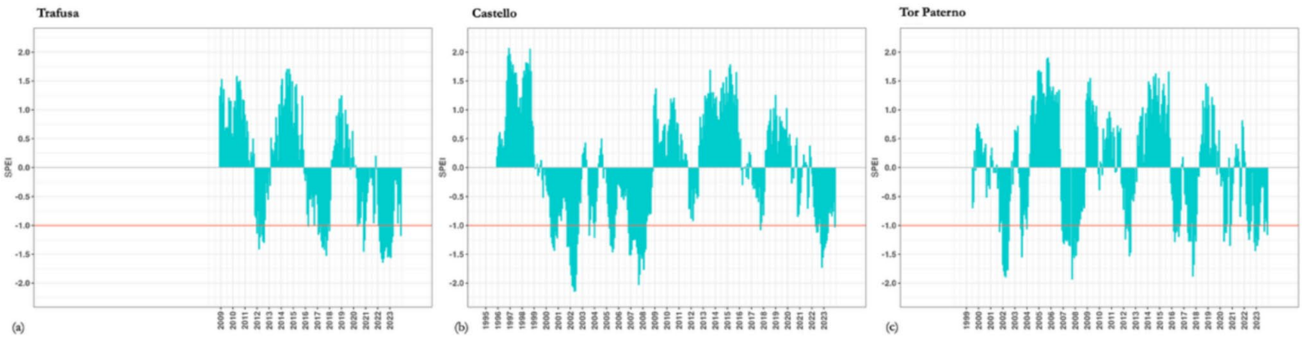

Fig. 12 Time series of SPEI12 for the Castelporziano meteorological stations of (**a**) Trafusa, (**b**) Castello, and (**c**) Tor Paterno

Table 6 Most relevant results of the ETCCDI indices for CPE meteorological stations from 2008 to 2023

Location	Index	Year	Maximum Value
Trafusa	WSDI-TX	2022	56 days
Castello	WSDI-TX	2022	51 days
Tor Paterno	WSDI-TX	2022	54 days
Trafusa	SU	2022	171 days
Castello	SU	2011, 2023	148 days
Tor Paterno	SU	2023	137 days
Trafusa	TR	2022	84 days
Castello	TR	2015	46 days
Tor Paterno	TR	2015	17 days
Trafusa	R20	2014	20 days
Castello	R20	2014	22 days
Tor Paterno	R20	2014	18 days
Trafusa	CDD	2008	86 days
Castello	CDD	2008	86 days
Tor Paterno	CDD	2009	106 days

Table 7 Trend of annual and seasonal ETCCDI for Castello and Tor Paterno meteorological stations. Trend computed from Castello data in the time window 1995–2023 (29 years); trend computed from Tor Paterno data in the time window 1999–2023 (25 years)

Location	Index	*P*-value	Trend	Period	Units
Tor Paterno	TXx	0.070	2.9**	YEAR	°C
Tor Paterno	TXx	0.038	2.5***	SON	°C
Tor Paterno	SU	0.002	32.8***	YEAR	days
Tor Paterno	SU	0.063	11.5**	JJA	days
Castello	SU	0.059	8.2**	JJA	days
Tor Paterno	SU	0.002	14.5***	SON	days
Tor Paterno	WSDI-TX	0.008	34.6***	YEAR	days
Castello	WSDI-TX	0.092	3.1**	SON	days
Castello	TR	0.001	21.4***	YEAR	days
Castello	TR	0.001	21.3***	JJA	days
Tor Paterno	WSDI-TN	0.037	28.6***	YEAR	days
Castello	WSDI-TN	0.016	27.6***	YEAR	days
Castello	CWD	0.014	5.0***	YEAR	days
Castello	CWD	0.046	2.6***	DJF	days

**P value < 0.10, ***P value < 0.05

Furthermore, at *Trafusa*, where data collection began in 2008, the recorded drought episodes align with those at *Tor Paterno,* namely in 2012, 2017–2018, and 2022–2023, along with an additional episode in the winter of 2021.

3.5 Trend analysis of extreme events

The assessment of climate change encompasses not only the average values of climatic variables but also their statistical distributions and extreme values. For this reason, we conducted a trend analysis on climate extreme indices. The results indicated statistically significant trends only in some instances related to temperature, while trends related to precipitation were rare. The indices used for temperature and precipitation are selected from the ETCCDI and listed in Tables 2 and 3 (Section 2.4), respectively. Likewise, in the case of averaged temperature and cumulated precipitation, the trend was not calculated for *Trafusa* due to the few years available in the historical series (2008–2023). However, the extreme indices were calculated, as well. For the *Castello* and *Tor Paterno* stations, we analyzed 29 and 25 years of data, respectively, to determine the trends in extreme indices. In Table 6, we present the maximum values recorded at the three weather stations: *Trafusa, Castello*, and *Tor Paterno*, for various extreme indices. This comparison is valid as we focused our analysis on the period from 2008 to 2023, corresponding to the duration of the shortest available time series, which is for *Trafusa*. For all three locations, the longest warm spell measured by T_{max} (WSDI-TX) occurred in 2022. Notably, *Trafusa* also experienced the highest number of days with maximum temperatures exceeding 25 °C (SU), totalling 171 days. Additionally, *Trafusa* recorded more tropical nights (TR) than the other locations, with 84 days compared to 46 days at *Castello* and 17 days at *Tor Paterno*. Regarding precipitation, the maximum number of days with extreme precipitation (R20) was observed in 2014 across all three stations. The longest dry spells (CDD) were noted in 2008 for *Trafusa* and *Castello*, while *Tor Paterno* had its longest dry spell in 2009. Furthermore, the dry spell recorded at *Tor Paterno* was significantly longer, lasting 106 days, compared to 86 days at the other two locations.

The results from the trend analysis are summarized in Table 7, which shows a general warming trend. As previously mentioned, the definitions of each index included in the table can be found in Section 2.4. The total variation for the years 1995 to 2023 is reported for both *Castello* and *Tor Paterno* in the "Trend" column. It is important to evaluate these variations in relation to the units of measurement for each index, which are listed in the "Units" column. Unlike the trend analysis shown in Table 4, we have allowed the trend estimates to be statistically significant up to a *P*-value threshold of 0.10 rather than 0.05. This adjustment increases the likelihood of incorrectly identifying a trend; however, it allows for a more comprehensive understanding of the overall situation. As a result, in Table 7, three asterisks are used to indicate *P*-values less than 0.05, while two asterisks represent *P*-values less than 0.10.

In detail, while the maximum value of daily maximum temperatures (*T*Xx) is increasing in *Castello*, *Tor Paterno*, and *Trafusa*, a significant trend is observed only for *Tor Paterno*, which has experienced an increase of +2.9 °C from 1995 to 2023. This increase is particularly pronounced during the autumn season. The number of days per year with maximum temperatures exceeding 25 °C (SU) is higher in *Trafusa* and *Castello* compared to *Tor Paterno*. However, *Tor Paterno* is the only station that shows a statistically significant upward trend, with an increase of +32.8 days from 1995 to 2023. Additionally, at *Tor Paterno*, a statistically significant increase of +34.6 days was noted in the Warm Spell Duration Index (WSDI-TX), which measures the number of days in the year with maximum temperatures above the 90th percentile for at least six consecutive days.

The longest warm spell recorded at *Tor Paterno* occurred in 2003, lasting 79 days. In recent years, the longest duration was observed at the *Trafusa* station in 2022, with 56 consecutive days of high temperatures.

In terms of minimum temperature, two indices were calculated: (a) tropical nights (TR), defined as the number of days with a minimum temperature exceeding 20 °C; and (b) heat waves (WSDI-TN), which represent the number of days in a year with a minimum temperature above the 90th percentile for at least six consecutive days.

The first observation from counting tropical nights (TR) is the significant difference between *Tor Paterno*, which consistently records fewer than 18 days, and *Trafusa*, which has shown values exceeding 60 days over the last 5 years (2019–2023), peaking at 84 days in 2022. The only station exhibiting a statistically significant upward trend is *Castello*, which has seen an increase of 21 tropical nights from 1995 to 2023.

The heat wave index (WSDI-TN), similar to the TR index, indicates a longer duration at the *Trafusa* and *Castello* stations compared to the *Tor Paterno* station. However, both *Castello* and *Tor Paterno* show a statistically significant increase in duration, with increases of 27.6 and 28.6 days since 1995 and 1999, respectively.

In contrast to the trends observed in temperature indices, the trends in precipitation indices are not statistically significant. When analyzing specific indices for the three stations, such as Rx1d and Rx5d—which represent the maximum precipitation values over 1 day and 5 days, respectively—no significant spatial differences were found. However, at the *Castello* station, there is a notable trend in the CWD index, which measures the maximum number of consecutive days with precipitation greater than 1 mm. Since 1995, this index has shown a significant increase of 5 days, particularly during the winter season.

4 Discussion and conclusion

This paper presents a climate analysis of the CPE in central Italy. It focuses on a trend analysis of temperature and precipitation, using both annual and seasonal data. The period of analysis spans from 1981 to 2022.

The analysis of all datasets indicates an increasing trend in temperatures (both T_{min} and T_{max}) on a seasonal scale, observed in the CPE as well as in surrounding urbanized regions.

Evaluating data from three stations within the CPE—*Trafusa*, *Castello*, and *Tor Paterno*—reveals a thermal gradient from the coastline (*Tor Paterno*) toward the interior (*Trafusa*). This gradient is evident in both annual and seasonal average temperature values, particularly for T_{min}. Another result of the analysis is that during the summer months (JJA), particularly in recent years, the positive thermal anomaly in the urbanized area of Rome is significantly higher than that in the CPE.

Conversely, the analysis of precipitation data indicates no significant trends. This lack of trends may be attributed to high interannual variability and the limited time-frame of the available data. Nonetheless, within the constraints of the analysis period, a consistent precipitation pattern across the CPE is apparent, remaining relatively stable throughout the year.

Besides, a joint analysis of precipitation and temperature reveals that, along the period 1995–2023, the last years (from 2014 to 2023) are all marked as the hottest and driest or hottest and most humid. Furthermore, the results show consistent drought patterns, with some unique occurrences at each station. In the middle part of the CPE, two drought episodes occurred from 2000 to 2003. A shorter one happened in the winter of 2004 and the summer of 2005. Two longer droughts lasted from 2007 to 2008 and from 2022 to 2023. On the coast, droughts were recorded in 2002–2003, 2007–2008, and 2022–2023, while, unlike the middle part, 2005 resulted in plenty of available water. Furthermore, the coast experienced droughts not noted in the middle: summer 2012, summer and part of autumn 2016, and summer, autumn, and winter 2017–2018. At the interior part of the CPE, where data collection started in 2009, droughts matched those registered on the coast in 2012, 2017–2018, 2022–2023, plus one in winter 2021.

This study examines indices related to climate extremes, highlighting a significant increase in tropical nights and a longer duration of warm spells for maximum temperatures. In the middle part of the CPE, the number of tropical nights has risen by 21 days from 1995 to 2023, while locations near the coast appear to benefit from the sea's nocturnal breeze, resulting in a very low number of tropical nights recorded by the weather station. Furthermore, the number of days per year with maximum temperatures above 25 °C in locations along the coast has increased by 33 days since 1999, and the duration of warm spells is now 35 days longer than in 1999.

Understanding the variations in climate variables and extreme weather events is crucial for assessing the impacts of climate change on ecosystems. This study analysed in detail the climate in the CPE area, using datasets collected by the internal monitoring network, from close by long-term meteorological stations and the ERA5L gridded dataset, demonstrating the importance of long-term measurement and analysis in revealing patterns and trends. Possibly, the warming trend and the consistent drought patterns identified by this study can be among the causal factors affecting the vegetation of CPE.

Author contributions Edmondo Di Giuseppe1, Sara Quaresima1*, Giorgio Matteucci1, Carlotta Ferrara2, Tiziano Sorgi2, Valerio Moretti2, Piermaria Corona2, Massimiliano Pasqui1 1* CNR, Institute of BioEconomy, Via dei Taurini 19, Rome, 00185, Italy. 2CREA, Research Centre for Forestry and Wood, Via Valle della Quistione, Rome, 00166, Italy.*Corresponding author(s). E-mail(s): sara.quaresima@cnr.it ; Contributing authors: edmondo.digiuseppe@cnr.it ; giorgio.matteucci@cnr.it ; carlotta.ferrara@crea.gov.it ; tiziano.sorgi@crea.gov.it ; valerio.moretti@crea.gov.it ; piermaria.corona@crea.gov.it ; massimiliano.pasqui@cnr.it; E.D.G. and S.Q. equally contributed to this work. E.D.G. Writing – review & editing, Writing – original draft, Visualization, Validation, Methodology, Formal analysis, Data curation, Conceptualization. S.Q. Writing – review & editing, Writing – original draft, Visualization, Validation, Methodology, Formal analysis, Data curation, Conceptualization. G.M. Writing – review & editing, Validation, Resources, Conceptualization. C.F. Writing – review & editing, Visualization, Data curation. T.S. Writing – review & editing, Data curation. V.M. Writing – review & editing, Data curation. P.C. Writing – review & editing, Data curation. M.P. Writing – review & editing, Writing – original draft, Validation, Formal analysis, Data curation, Conceptualization.

Data availability Three datasets were analysed during the current study: (1) the Castelporziano Presidential Estate Monitoring Network (CPE), (2) the Italian Air Force Meteorological Service (AM), and (3) the ERA5-Land gridded reanalysis (ERA5L). ERA5-Land is available at https://cds.climate.copernicus.eu/datasets.

Declarations

Conflict of interests The authors declare no competing interests.

References

Armenia S, Bellomo D, Medaglia CM, Nonino F, Pompei A (2021) Water resource management through systemic approach: the case of Lake Bracciano. J Simul 15(1–2):65–81. https://doi.org/10.1080/17477778.2019.1664266

Baldi M, Dalu G, Maracchi G, Pasqui M, Cesarone F (2006) Heat waves in the Mediterranean: a local feature or a larger-scale effect? Int J Climatol 26(11):1477–1487. https://doi.org/10.1002/joc.1389

Beguería S, Vicente-Serrano SM (2023) SPEI: calculation of the standardized precipitation-evapotranspiration index. R package version 1.8.1. https: //CRAN.R- project.org/package=SPEI

Bronaugh D, Schoeneberg A (2023) Zyp: Zhang + Yue-Pilon Trends Package v0.11-1. R package. https://cran.r-project.org/package=zyp

Buuren S (2007) Multiple imputation of discrete and continuous data by fully conditional specification. Stat Med Res 16(3):219–242. https://doi.org/10.1177/0962280206074463

Centers for Disease Control and Prevention (CDC) (2004) Impact of heat waves on mortality—Rome, Italy, June–August 2003. MMWR Morb Mortal Wkly Rep 53(17): 369–371

Copernicus Climate Change Service (2019) ERA5-Land Hourly Data from 2001 to Present. ECMWF. https://doi.org/10.24381/CDS.E2161BAC.

D'Ippoliti D, Michelozzi P, Marino C, de'Donato F, Menne B, Katsouyanni K, Kirchmayer U, Analitis A, Medina-Ramón M, Paldy A, Atkinson R, Kovats S, Bisanti L, Schneider A, Lefranc A, Iñiguez C, Perucci CA (2010) The impact of heat waves on mortality in 9 European cities: results from the EuroHEAT project 9(1): 37. https://doi.org/10.1186/1476-069X-9-37. Accessed 21 February 2025

Di Giuseppe E, Pasqui M, Magno R, Quaresima S (2019) A counting process approach for trend assessment of drought condition. Hydrology. https://doi.org/10.3390/hydrology6040084

Dono G, Cortignani R, Dell'Unto D, Deligios P, Doro L, Lacetera N, Mula L, Pasqui M, Quaresima S, Vitali A, Roggero PP (2016) Winners and losers from climate change in agriculture: insights from a case study in the mediterranean basin. Agric Syst 147:65–75. https://doi.org/10.1016/j.agsy.2016.05.013

Gottlieb AR, Mankin JS (2024) Evidence of human influence on Northern hemisphere snow loss. Nature 625(7994):293–300. https://doi.org/10.1038/s41586-023-06794-y
Hampel FR (1974) The influence curve and its role in robust estimation. J Am Statist Assoc 69(346): 383–393. Accessed 6 March 2025
Hargreaves GH (1994) Defining and using reference evapotranspiration. J Irrig Drain Eng 120(6):1132–1139. https://doi.org/10.1061/(ASCE)0733-9437(1994)120:6(1132)
Hijmans RJ (2023) Terra: spatial data analysis. https://rspatial.org/
IPCC (2023) Climate change: synthesis report. In: Core Writing Team, Lee H, Romero J (eds) Contribution of working groups I, II and III to the Sixth Assessment Report of the Intergovernmental Panel on Climate Change, IPCC, Geneva, Switzerland, pp 35–115. https://doi.org/10.59327/IPCC/AR6-9789291691647.
Masson-Delmotte V, Zhai P, Pirani A, Connors SL, Péan C, Berger S, Caud N, Chen Y, Goldfarb L, Gomis MI, Huang M, Leitzell K, Lonnoy E, Matthews JBR, Maycock TK, Waterfield T, Yelek¸ci Ò, Yu R, Zhou B (2021) Climate change 2021: the physical science basis. Contribution of working group I to the sixth assessment report of the Intergovernmental Panel on Climate Change. Cambridge University Press, Cambridge, United Kingdom and New York, NY, USA. https://doi.org/10.1017/9781009157896
MedECC (2020) Climate and environmental change in the Mediterranean basin—current situation and risks for the future. First Mediterranean assessment report. https: //doi.org/10.5281/zenodo.4768833
Monteiro M, Costa M (2023) Change point detection by state space modeling of long-term air temperature series in Europe. Stats 6(1):113–130. https://doi.org/10.3390/stats6010007
Muñoz-Sabater J, Dutra E, Agustí-Panareda A, Albergel C, Arduini G, Balsamo G, Boussetta S, Choulga M, Harrigan S, Hersbach H, Martens B, Miralles DG, Piles M, Rodríguez-Fernández NJ, Zsoter E, Buontempo C, Thépaut J-N (2021) ERA5-land: a state-of-the-art global reanalysis dataset for land applications. Earth Syst Sci Data 13(9):4349–4383. https://doi.org/10.5194/essd-13-4349-2021
Nardone A, Bonella G, Cecca D, Cimini D (2025) Effect of abiotic components on Castelporziano environment. In press in this issue
Panagiotopoulos F, Shahgedanova M, Hannachi A, Stephenson DB (2005) Observed trends and teleconnections of the Siberian high: a recently declining center of action. J Climate 18(9):1411–1422. https://doi.org/10.1175/JCLI3352.1.Chap.JournalofClimate
Pasqui M, Di Giuseppe E (2019) Climate change, future warming, and adaptation in Europe. Anim Front 9(1):6–11. https://doi.org/10.1093/af/vfy036
Pignatti S, Capanna E, Porceddu E (2015) Castelporziano, research and conservation in a Mediterranean forest ecosystem: presentation of the volume. Rend Fis Acc Lincei 26(3):265–266. https://doi.org/10.1007/s12210-015-0463-9
Reig-Gracia F, Vicente-Serrano SM, Dominguez-Castro F, Bedia-Jiménez J (2021) Clim Ind: Climate Indices. R package version 0.1-3. https://CRAN.R-project. org/package=ClimInd
Sappa G, Ferranti F, De Filippi FM, Iacurto S (2019) Recent drought effects on Bracciano lake water availability, 19:3, pp 457–464. 19th International Multidisciplinary Scientific Geoconference, SGEM 2019. https://doi.org/10.5593/sgem2019/3.1/S12.059.
Schafer JL (1997) Analysis of incomplete multivariate data, 1st edn. Chapman and Hall/CRC. https://doi.org/10.1201/9780367803025
Sen PK (1968) Estimates of the regression coefficient based on Kendall's Tau. J Am Statist Assoc 63(324): 1379–1389. https://doi.org/10.2307/2285891 2285891
Tukey JW (1949) Comparing individual means in the analysis of variance. Biometrics 5(2): 99–114. Accessed 6 March 2025
van Buuren S, Groothuis-Oudshoorn K (2011) Mice: multivariate imputation by chained equations in R. J Stat Softw 45(3):1–67. https://doi.org/10.18637/jss.v045.i03
Ventura M, Careddu G, Calizza E, Sporta Caputi S, Argenti E, Rossi D, Rossi L, Costantini ML (2023) When climate change and overexploitation meet in volcanic lakes: the lesson from Lake Bracciano, Rome's strategic reservoir. Water 15(10):1959. https://doi.org/10.3390/w15101959
Vicente-Serrano SM, Beguería S, López-Moreno JI (2009) A multiscalar drought index sensitive to global warming: the standardized precipitation evapotranspiration index. J Clim 23(7):1696–1718. https://doi.org/10.1175/2009JCLI2909.1
von Storch H (1999) Misuses of statistical analysis in climate research. In: von Storch H, Navarra A (eds) Analysis of climate variability. Springer, Berlin, Heidelberg, pp 11–26. https://doi.org/10.1007/978-3-662-03744-72
Zhang X, Vincent LA, Hogg WD, Niitsoo A (2000) Temperature and precipitation trends in Canada during the 20th century. Atmos-Ocean 38(3):395–429. https://doi.org/10.1080/07055900.2000.9649654